Magneto-Electric Interactions in Composites of Self-Biased Y- and W-type Hexagonal Ferrites and Lead Zirconate Titanate: Experiment and Theory

Ying Liu,[1,2] Jitao Zhang,[1,3] Peng Zhou,[1,2] Cunzheng Dong,[4] Xianfeng Liang,[4] Wei Zhang,[1] Tianjin Zhang,[2] Nian X. Sun,[4] Dimitry Filippov,[5] and G. Srinivasan[1]*

[1]*Departmentof Physics, Oakland University, Rochester, MI 48309-4401, USA*

[2]*Department of Materials Science and Engineering, Hubei University, Wuhan 430062, China*

[3] *College of Electrical and Information Engineering, Zhengzhou University of Light Industry, Zhengzhou 450002, China*

[4]*Department of Electrical and Computer Engineering, Northeastern University, Boston, Massachusetts 02115, USA*

[5]*Novgorod State University, Veliky Novgorod, 173003 Russia*

ABSTRACT

This report is on the observation and theory for strong mechanical strain mediated magneto-electric (ME) coupling in composites of lead zirconate titanate (PZT) and self-biased Y- or W-type hexagonal ferrites. Polycrystalline Y-type, $(Ni_{1-x}Zn_x)_2$ Y, and W-types, $(Co_{1-x}Zn_x)_2$ W, hexagonal ferrites for x = 0-0.4 prepared by ceramic processing techniques showed a large remnant magnetization due to uniaxial or in-plane magneto-crystalline anisotropy. The strength of ME coupling in symmetric trilayer composites of the ferrites and PZT was measured by ME voltage coefficient (MEVC) at low-frequency and at longitudinal electro-mechanical resonance (EMR). The bias magnetic field H dependence of MEVC at low-frequency in the composites with (Ni,Zn) Y showed hysteresis with its value under self-bias 90% or more of the value for optimum bias field. In the case of composites with W-type ferrites, the MEVC under zero-external bias was 60-80% of its value for optimum bias field. Both types of composites when subjected to an ac

magnetic field at EMR frequency showed an order of magnitude enhancement in the MEVC compared to low-frequencies and the peak value at EMR for zero bias was 90% of its value under optimum bias. A model has been developed for the large ME response under the self-bias provided by the remnant magnetization and estimated values of MEVC are in good agreement with the data. The hexaferrite-ferroelectric composites showing ME response without the need for an external magnetic bias are of importance for use as sensors and sensor arrays of magnetic fields.

- Corresponding author: Gopalan Srinivasan

  Email:srinivas@oakland.edu

1. INTRODUCTION

Single-phase or composite materials with long range ordering of magnetic and electric dipoles are multiferroic and are of importance for studies on the physics of interaction between the magnetic and electric subsystems [1-4] and for applications in advanced technologies including sensors and high frequency devices [5-7]. In the case of two-phase composites consisting of ferromagnetic and ferroelectric phases it is possible to realize very strong magneto-electric (ME) coupling with proper choice for the ferroic phases [8-10]. The ME interaction in this case is a product-property that arises from magnetostriction in the ferromagnetic phase in an applied magnetic field H and the resulting ferroelectric polarization due to piezoelectric effect in the ferroelectric phase [11]. The electrical response to H is termed direct-ME effect (DME). Similarly, the mechanical deformation in the ferroelectric phase in an applied electric field E is expected to manifest as a change in the magnetization or anisotropy field in the ferromagnetic phase and is termed converse-ME effect (CME). Composites with 3d-transition metals or rare-earth metals or alloys, spinel ferrites, and manganites for the ferromagnetic phase and barium titanate, lead zirconate titanate (PZT) and lead magnesium niobate-lead titanate (PMN-PT) were studied extensively in recent years [3-10].

The strength of DME in composites could be determined by subjecting the sample to AC and/or DC magnetic fields and measuring the changes in ferroelectric order parameters such as the polarization or permittivity [12]. A technique of particular interest in this regard for applications in magnetic sensors is the measurement of ME voltage coefficient (MEVC) that involves applying a bias field H and an AC magnetic field h to the sample [6,13]. The induced ME voltage v in the sample is then measured for estimation of MEVC = $v/(h\,t)$ where t is the composite (or ferroelectric layer) thickness. The MEVC is directly proportional to the product of the piezomagnetic

coefficient $q = d\lambda/dH$, where λ is the magnetostriction, and d/ε where d is the piezoelectric coupling coefficient and ε is the permittivity. The MEVC, therefore, can be considered as an intrinsic parameter that is a measure of the strength of ME coupling between the ferroic phases. For comparison of ME responses amongst ferroic composites, however, it is necessary consider the influence of demagnetizatizion on the magnitude of λ and q and similar effects of an electric field on ferroelectric order parameters. Thus the shape and geometry of the composites do have an effect on the magnitude of MEVC. A giant low frequency ME effect with MEVC as high as 10 V/(cm Oe) was reported in several composites [13]. A significant enhancement in MEVC occurs when h is applied at frequencies corresponding to electromechanical resonance (EMR) in the composite [7]. A key ingredient for achieving a large MEVC in the composites is the application of a bias magnetic field H since the piezomagnetic coefficient $q \sim 0$ for $H = 0$ for most of the ferromagnets [7,13]. Several avenues were explored for achieving a large MEVC under zero external bias. These include the use of functionally graded ferromagnetic layers in the composites [7]. Grading the magnetization or compositionally graded ferromagnetic phases were reported to result in an induced magnetic field that acted as the necessary bias field and gave rise to strong ME coupling under H=0 [14-17].

This work is aimed at achieving a large zero-field ME coupling in a composite with a ferrite in which a large remnant magnetization that could potentially act as an internal magnetic field. Spinel ferrites, in general, have a cubic anisotropy and therefore a rather small magnetocrystalline anisotropy field and remnant magnetization. Hexagonal ferrites with very high anisotropy fields are potentially useful for use in composites showing high zero-field ME response. Hexaferrites consisting of spinel and hexagonal blocks are ferrimagnets with the Curie temperature ranging from 700 K to 900 K and high anisotropy field H_A [18,19]. Based on the arrangement of spinel and

hexagonal blocks in the crystallographic structure, the ferrites are classified into M-, U-, W-, X-Y-, and Z-type, with either uniaxial or in-plane anisotropy field. Iron ions occupy sites with octahedral, tetrahedral and trigonal coordination and antiferromagnetic alignment of Fe^{3+} in these sites results in a net ferromagnetic moment and spin-orbit coupling amongst Fe ions results in uniaxial or in-plane anisotropy field H_A as high as 20 kOe [18]. In a polycrystalline hexaferrite the high anisotropy field will result in a large remnant magnetization which could act as self-magnetic bias in a composite with a ferroelectric, leading to a large MEVC in the absence of an external bias. M-type ferrites are not considered in this study due to low λ-values and weak ME coupling reported for layered composites with PZT [20]. For this study we choose Y- and W-type hexaferrites a large anisotropy field as well as high magnetostriction [18-20]. Y-type ferrites $Ba_2 Me_2 Fe_{12} O_{22}$ (Me_2Y with Me = Ni, Fe, ..) have high λ and q. Ni_2Y shows uniaxial anisotropy field $H_A \sim 14$ kOe and, in particular, has high q. The magnetic order parameters in Y-type ferrite could be controlled with nonmagnetic substitutions such as Zn. In Zn_2Y, when Ni is completely replaced by Zn, both H_A and λ decrease [21,22]. But for partial substitution of Zn for Ni, the piezomagnetic coefficient q, a key ingredient for strong ME coupling, shows an increase. Therefore we choose Y-type ferrite $(Ni,Zn)_2Y$, $Ba_2(Ni_{1-x} Zn_x)_2 Fe_{12}O_{22}$, with x = 0-0.4 for the present study. Similarly W-type ferrites with the composition $Ba Me_2 Fe_{16} O_{27}$ (Me_2W with Me = Co and/or Zn) are also of interest for the study. Zn_2W has (uniaxial) H_A = 12.5 kOe whereas Co_2W has in-plane H_A = -21 kOe and high λ-value. Zn-substitution for Co will allow for control of both λ and H_A, from in-plane anisotropy to uniaxial anisotropy [21-24]. W-type of the composition $Ba (Co_{1-x} Zn_x)_2 Fe_{16} O_{27}$ (x=0-0.4) was used for composites in this study. Zn-substitutions in excess of 0.4 result in significant reduction in λ in both systems.

Polycrystalline (Ni,Zn) Y and (Co, Zn) W were prepared by ceramic processing techniques and were characterized in terms of structural and magnetic parameters. Vendor (American Piezo Ceramics) supplied PZT (APC 850) with the approximate composition $Pb\ Ti_{0.52}\ Zr_{0.48}\ O_3$ and with unknown substitutions and d_{31} = -175 pm/V was used for the ferroelectric phase in our composites.

Symmetric trilayer composites of ferrite- PZT-ferrite were made by epoxy bonding. The strength of ME interactions was measured by MEVC at low-frequency and at electromechanical resonance. We measured strong ME coupling for both Y- and W-type hexaferrites systems in composites with PZT. The overall coupling strength in composites with (Ni, Zn)Y is found to be much stronger than in W-type hexaferrites and PZT. The zero-bias MEVC at low frequencies and at EMR in some of the Y-type ferrite based composites is ~ 90% of the MEVC under optimum bias. A model for ME coupling under self-bias has been discussed and the estimated values of ME voltage coefficients are in very good agreement with data. The results of the studies are of interest for use of the composites in magnetic sensors [25-27] and energy harvesting technologies [28,29]. Details of our studies are provided in the sections that follow.

2. Experiment

Y-type ferrites, $Ba_2\ (Ni_{1-x}\ Zn_x)_2\ Fe_{12}\ O_{22}$with x = 0 to 0.4 in steps of 0.1, and W-type hexagonal ferrites, Ba $(Co_{1-x}Zn_x)_2\ Fe_{16}\ O_{27}$ with x = 0, 0.2 and 0.4 were prepared by traditional ceramic processing techniques. Appropriate amounts of oxides or carbonates of Ba, Ni, Zn, Fe and Co were mixed in a ball-mill for several hours, followed by presintering at 800 C for 6 hrs. The presintered powder was then ball-milled for 24 hrs. A polyvinyl alcohol-based binder was added to dried powder and then pressed into blocks of dimensions 45 mm × 15 mm × 7 mm. Final sintering was carried out at 1225-1275 C for 6 hrs. It was necessary to set the heating and cooling

rates to 1 C/min in order to avoid surface cracks, blowholes and similar defects in the sintered ferrite blocks.

The ferrites were characterized by x-ray diffraction (XRD). Room temperature magnetization versus *H* data were obtained on thin rectangular platelets with a vibrating sample magnetometer (VSM). Magnetostriction, a key parameter that determines the strength of ME coupling, was measured with a strain gage and a strain indicator. For fabrication of composites with PZT, rectangular platelets of dimensions 35 mm × 5 mm × 0.5 mm were cut from the ferrite blocks. Vendor supplied pre-poled PZT (American Piezo Ceramics #850) platelets of dimensions 40 mm × 5 mm × 0.5 mm were used. Ferrite-PZT-ferrite trilayers were made by bonding the platelets with a 2-part epoxy (M-bond 600, Micro Measurements Inc). The epoxy layers were 2 μm in thickness and cured at 125 C for 45 min. Studies on ME coupling were done at low-frequencies and at electromechanical resonance (EMR). The composite was subjected to a bias magnetic field *H* and an ac magnetic field *h*, with both fields parallel to each other and along the sample length. An electromagnet was used for applying *H* and a pair of Helmholtz coils for the ac field. Lock-in detection was used to measure the ME voltage *v* generated across the thickness *t* of PZT. The ME voltage coefficient (MEVC) = $v/(h\ t)$ was determined as a function of *H* and frequency *f* of the ac field.

3. Results

Representative XRD data for W- and Y-type ferrites are shown in Fig.1. The data show peaks belonging to either W- or Y-type ferrites and the samples are free of any impurity phases [30,31]. We discuss first magnetic and ferroelectric characterization of the ferrites and PZT. This is followed by results on the nature of ME interactions in the composites. Data on *M* vs *H* were obtained for in-plane fields either parallel to the length or width of rectangular platelets of the

samples and for *H* perpendicular to the sample plane. Figure 2 shows representative *M* vs *H* data for $(Ni,Zn)_2$ Y for Zn substitutions x = 0, 0.2, and 0.4. The results are for *H* along the sample length. A typical hysteresis with the saturation magnetization M_s increasing from 23 emu/g for x = 0 to 32.5 emu/g for x – 0.4 is observed in Fig.2. Past studies reported increase in room temperature M_s with Zn substitution, from 23.7 emu/g for Ni_2Y to 37.5 emu/g for Zn_2Y.

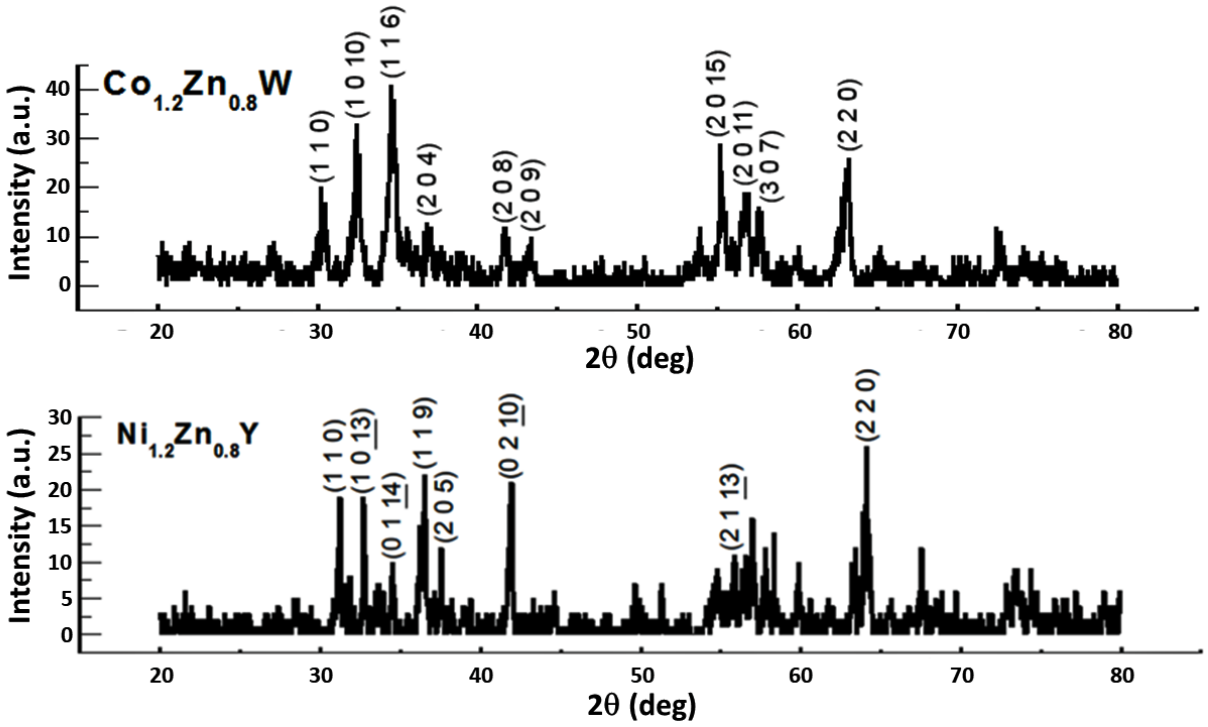

Fig.1. X-ray diffraction data for polycrystalline W- and Y-type hexagonal ferrites.

Such an increase in M_s is similar to the case of spinel ferrites such as $Me_{1-x}Zn_x\ Fe_2O_4$ (Me = Ni, Co…) and is attributed to Zn ion displacing Fe^{3+} and occupying the tetrahedral site in the spinel block of the hexaferrite, thereby increasing the net ferromagnetic moment [18]. The data in Fig.2 also shows an increase in the remnant magnetization M_r with Zn substitution, from 7 emu/g for Ni_2Y to 9 emu/g for $Ni_{1.2}\,Zn_{0.8}\,Y$.

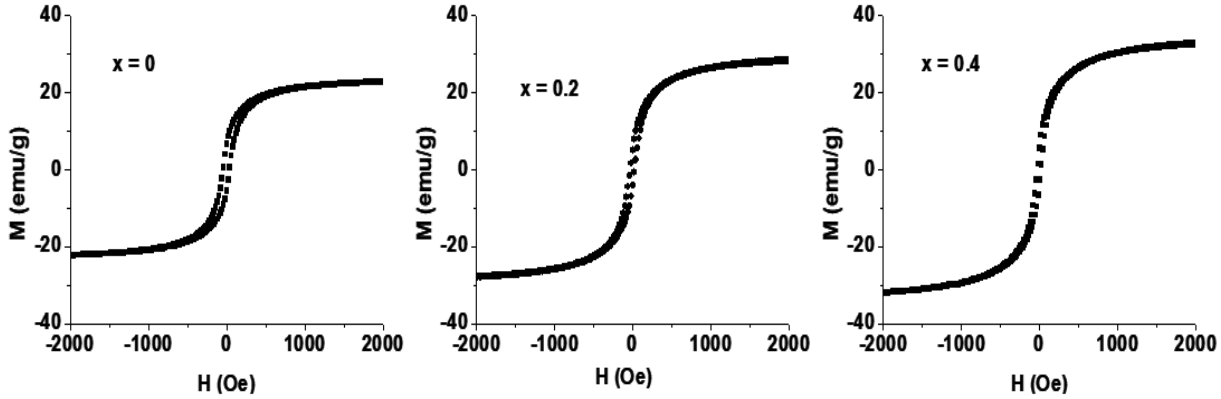

Fig.2. Room-temperature magnetization as a function of H for $(Ni_{1-x}Zn_x)_2$ Y. The field H was applied parallel to the plane of a rectangular platelet and along the sample length.

Similar *H*-dependence of *M* for $(Co_{1-x}Zn_x)_2$ W are shown in Fig.3 for in-plane *H* parallel to the length of the sample. Single crystal Co_2W has easy plane anisotropy and it becomes uniaxial anisotropy for high concentration of Zn substitution [18]. Our measurements on the polycrystalline samples showed a decrease in the *H*-value for saturation of *M* with increasing x and $M_s \sim 60$ emu/g for x=0 and 0.2. A decrease in M_s to 50 emu/g is measured for the sample with x = 0.4. These M_s values are in general agreement with reported values for polycrystalline $(Co,Zn)_2$ W [18, 32]. The M_r values estimated from Fig.3 are 8, 13, and 10 emu/g for x = 0, 0.2 and 0.4, respectively.

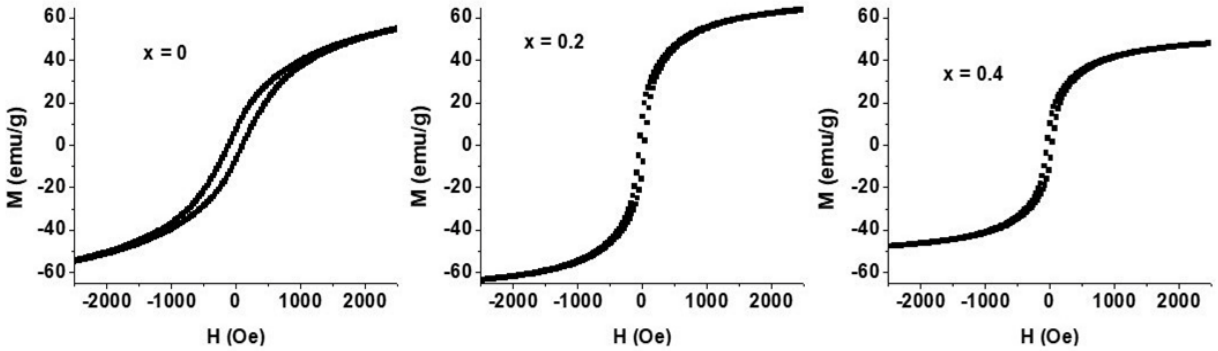

Fig.3. Similar room-temperature M vs H data for $(Co_{1-x}Zn_x)_2W$. The field H was applied parallel to the plane of a rectangular platelet and along the sample length.

The magnetostriction λ, an important parameter that determines the strength of the strain mediated ME coupling in a composite with PZT, was measured on rectangular platelets. With an in-plane H applied parallel to the sample length (direction-*1*), in-plane magnetostriction along the field direction, λ_{11}, and perpendicular to H, λ_{12} were measured as a function of H. Figure 4 shows such λ vs H data for both Y- and W-type hexaferrites. For $(Ni, Zn)_2Y$, $\lambda_{11}$is negative, increases in magnitude with H and attains saturation for $H > 1$ kOe. The magnetostriction λ_{12} is positive and its magnitude is approximately 50% of λ_{11} as expected. With the substitution of Zn, λ_{11} shows an increase for x = 0.1. Further increase in x results in a decrease in the magnitude of λ_{11}. For x = 0.4 the λ-values were quite small and are not shown in Fig.4. Figure 4 also shows λ vs H data for $(Co_{1-x}Zn_x)_2$ W for x = 0, 0.2 and 0.4. Saturation of magnetostriction is not observed for fields up to 1.2 kOe and λ is approximately equal for x=0 and 0.2 and shows a significant decrease for x = 0.4. The component λ_{12} shows a linear increase with increasing H and has insignificant dependence on x.

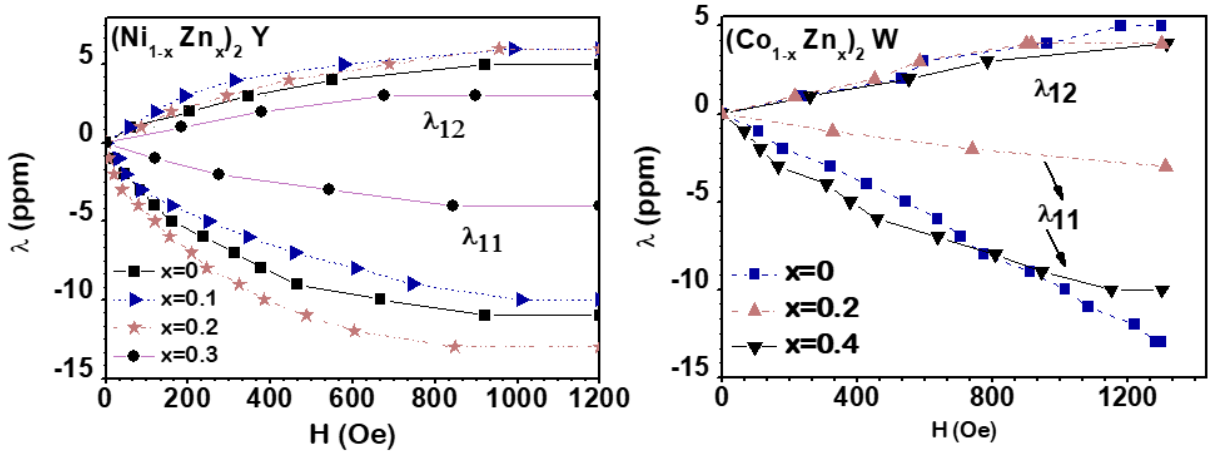

Fig.4. Room-temperature magnetostriction as a function of H measured parallel to the field direction (λ_{11}) and perpendicular to the field (λ_{12}) for (a) Y- and (b) W-type hexagonal ferrites.

The strengths of ME coupling in symmetric trilayers of hexaferrites and PZT were measured by MEVC at low frequencies and at longitudinal acoustic resonance. Figure 5 shows MEVC vs *H* for (Ni,Zn)Y – PZT composites for Zn substitution x = 0-0.4. The data are for *H* and ac field *h* = 1 Oe (at 30 Hz) parallel to the sample plane and along the length. For the composite with x=0, a sharp in MEVC to a maximum value of ~ 110 mV/cm Oe for *H* = 30 Oe is observed and is followed by a decrease in MEVC to a minimum of zero for *H* = 1.3 kOe. As *H* is decreased back to zero, MEVC is found to increase to a maximum slightly smaller than the peak value for increasing *H*. When *H* is reversed, MEVC also reverses sign and the negative sign indicates a 180 deg. phase change for the MEVC and its value stays the same as for +*H*. There is also a hysteresis in the MEVC vs *H* data. For composites with ferrites with higher Zn, a small decrease in the peak value of MEVC is measured for x = 0.1 and 0.2, but for x = 0.4, the MEVC drops to a peak value of 30 mV/cm Oe.

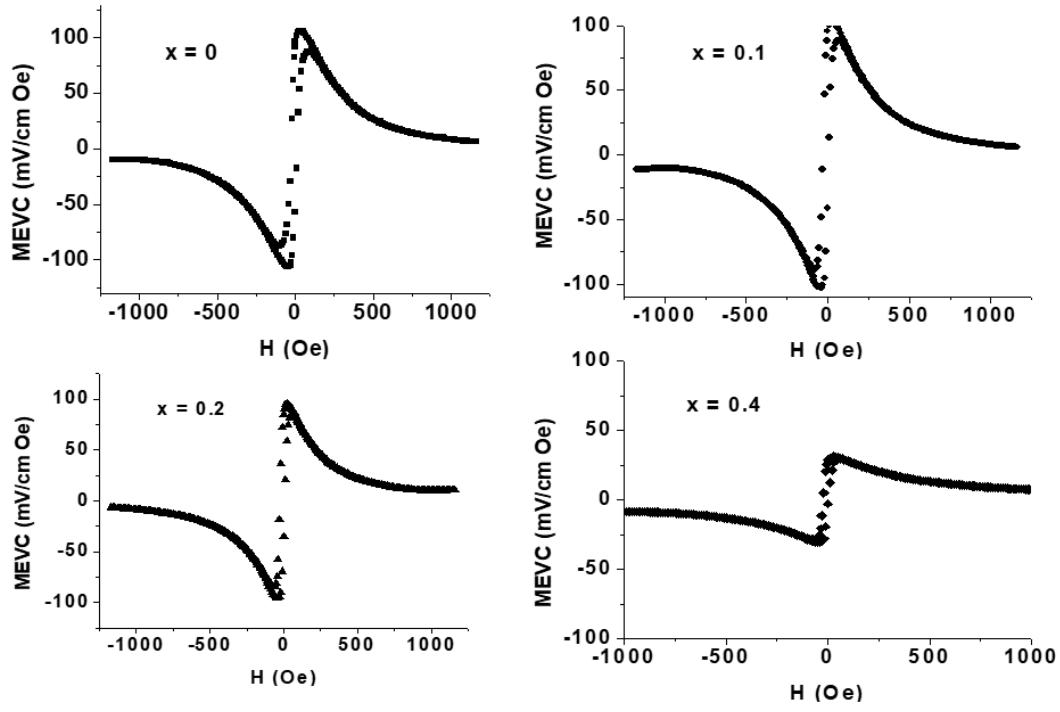

Fig.5. Low frequency ME voltage coefficient vs bias field H data for composites of $(Ni_{1-x}Zn_x)_2$ *Y and PZT.*

Similar *H*-dependence of low-frequency MEVC for trilayer composites with W-type ferrites are shown in Fig.6. For the sample with Co_2W (x=0), the MEVC is non-zero for $H = 0$, shows a slight increase with increasing *H* and has a constant value of 27 mV/cm Oe for $H > 300$ Oe. As *H* is decreased, MEVC decrease to zero for $H = 100$Oe, reverses sign, and attains a value of 18 mV/cm Oe for $H=0$. A hysteresis in MEVC vs *H* is evident in Fig.6 for composites with x = 0. When Zn is substituted in the W-type ferrite, the data in Fig.6 shows strengthening of ME response. The peak MEVC increases to 46 and 65 mV/cm Oe for x = 0.2 and 0.4, respectively. One also notices a decrease in MEVC for $H > 200$ Oe in the data for x = 0.2 and 0.4.

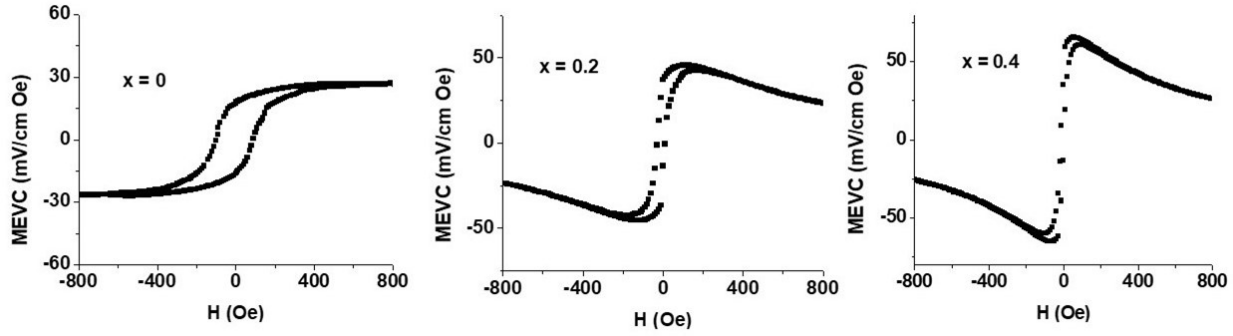

Fig.6. Low frequency ME voltage coefficient vs bias field H data for composites of $(Co_{1-x}Zn_x)_2W$ and PZT.

The most significant observation in Figs. 5 and 6 is the evidence for strong ME interactions under zero external bias field. Figure 7 shows the measured MEVC under $H = 0$ for composites with W- and Y-type ferrites and are compared with MEVC under optimum bias for maximum MEVC. The strength of DME is directly proportional to the piezomagnetic coefficient *q* which in general is vanishingly small for external bias $H = 0$. In the present case, however, the large remnant magnetization acts as self-biasing field and results in a large piezomagnetic coupling coefficient and strong ME interactions. Among the two systems studied here, composites with

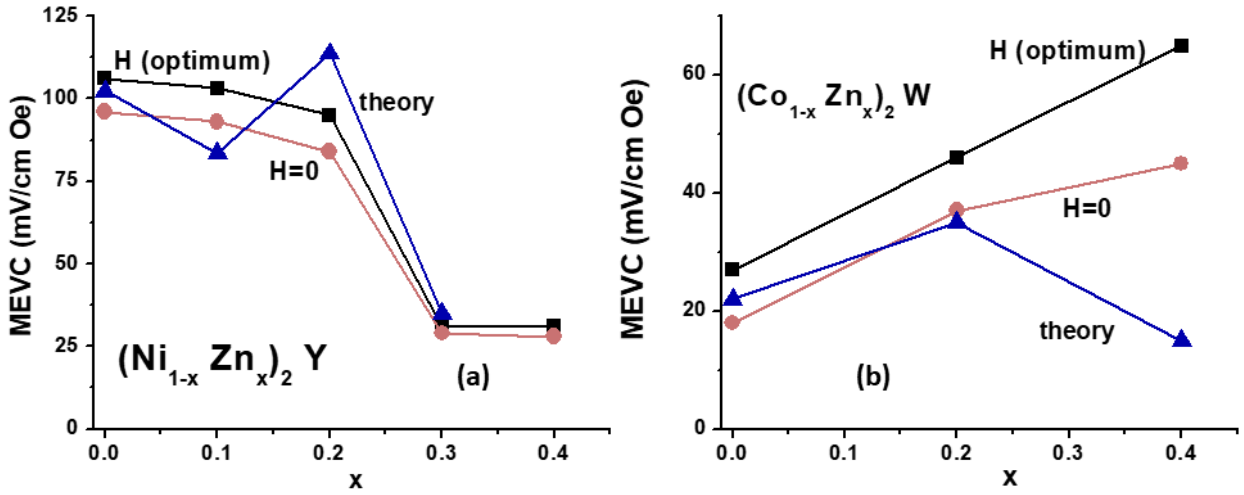

Fig.7. Maximum values of ME voltage coefficient and MEVC for zero bias field for composites of PZT and (a) Y-type or (b) W-type hexagonal ferrites. The MEVC values were obtained from data as in Figs. 5 and 6. Estimated values of MEVC under H = 0 are also shown.

(Ni, Zn)Y ferrites have the strongest the ME coupling under zero-bias with its value more than 90% of the MEVC under optimum bias for all the compositions studied. Samples with (Co,Zn)W-ferrites show a relatively weak ME interaction for H =0 with the MEVC in the range 55-81% of the value for optimum bias. According our model discussed in the following section the large MEVC under self-bias in these composites with the hexagonal ferrites is essentially due to uniaxial anisotropy and the resulting remnant magnetization in these ferrites.

We measured the frequency f dependence of the MEVC in the composites under two different conditions, (i) for H corresponding to maximum in MEVC and an ac field, both parallel to each other and along the length of the sample and (ii) for $H = 0$, and representative results for composites with Y- or W-type ferrites are shown in Fig.8. A resonance in MEVC vs f is observed and the peak in the ME coefficient occurs at the longitudinal acoustic mode frequency f_r. Under optimum bias H, the MEVC at f_r is higher by an order of magnitude or more compared to the low-frequency values in Fig.5 and 6. For $H = 0$, the MEVC for both composite systems shows a peak value at f_r

and its value is 90% of the value under optimum bias. For samples with Ni_2Y, the peak value of MEVC decreased with increasing Zn substitution whereas MEVC at f_r. increased with Zn-substitution for composites with the W-type. The resonance occurs at 50-60 kHz and the change in f_r. is mainly due to any variation overall length of the samples and their average density as discussed later.

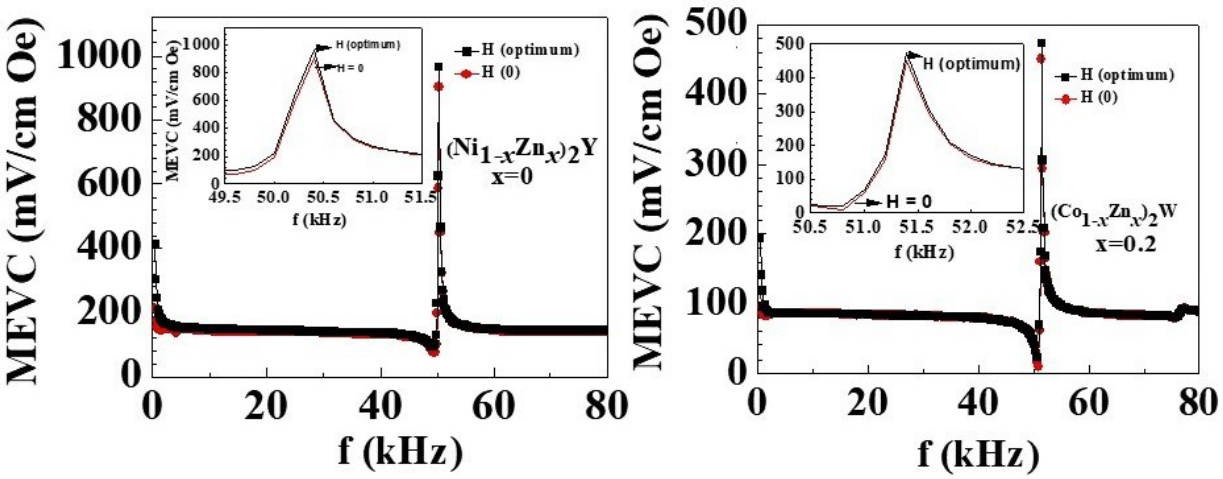

Fig.8. ME voltage coefficient vs frequency data for (left) Ni_2Y and PZT and (right) $(Co_{0.8}Zn_{0.2})_2W$ and PZT. The results are for (i) optimum H-value corresponding to maximum MEVC and for (ii) H =0. The insets show MEVC vs f on an expanded scale.

4. Model for ME effects under self-bias and Discussion

A model for the ME effects under self-bias is discussed next and is followed by discussion of the results. We consider a ferrite/PZT/ferrite trilayer ME composite structure and a coordinate system (X_1, X_2, X_3) = (*1,2,3*) as shown in Fig.9. The PZT is poled along the direction *3* and the composite is subjected to magnetic fields *H* and *h* parallel to its plane and along direction *1*. In this case, the upper and lower surfaces of the composite are equipotential surfaces, therefore, only the component of the electric field vector E_3 is nonzero. For PZT polarized along X_3 nonzero

component of piezoelectric tensor are the components $d_{31} = d_{32}$, d_{33} and $d_{15} = d_{24}$. Electric field along X_3 induces either tensile or compressive strains, and shear deformations will be absent in this case. Since the composite is symmetric, flexural vibrations will also be absent and we can restrict our consideration to the planar vibrations propagating along the longitudinal direction.

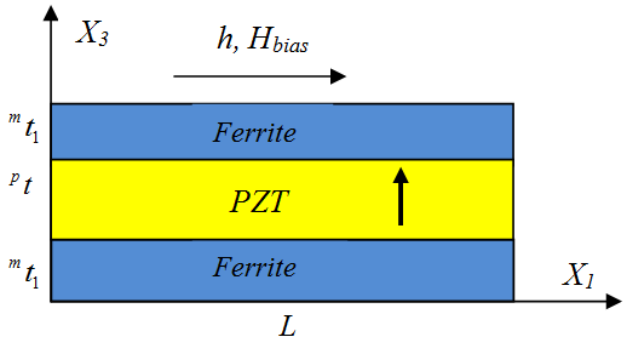

Fig.9. Cross-sectional view of trilayer ferrite-piezoelectric composite. The length L of trilayer in the (X_1, X_2) plane and its thickness along the X_3 axis. The ${}^{m}t = 2\,{}^{m}t_1$ and ${}^{p}t$ represent the total thickness of magnetostrictive layer and the thickness of piezoelectric layer, respectively. It is assumed that the PZT layer is polarized along X_3 axis. The ME effect was excited by magnetic field along X_1 and lead to resulting electric field along X_3 axis.

For ferrite layers we have to add the magnetostrictive term in the equation for strain. Magnetostriction is nonlinear function of magnetization. Near the equilibrium we can represent this function as a series using the relation:

$$\lambda(M) = \frac{1}{2}\frac{\partial^2 \lambda}{\partial M^2} M^2 + \ldots = \frac{1}{2} b M^2 + \ldots . \qquad (1)$$

Here $M = M_r + M(H)$ is magnetization, M_r is remnant magnetization, $M(H)$ is induced magnetization in external magnetic field $H = H_{bias} + h$, H_{bias} is bias magnetic field and h is ac magnetic field. For low magnetic fields, the magnetization can be represented as

$$M(H) = M_r + \chi(H)(H_{bias} + h), \quad (2)$$

where $\chi(H)$ is magnetic susceptibility. Substituting Eq.(2) into Eq.(1) we can represent λ as

$$\lambda(h) = qh + \frac{1}{2} gh^2 . \quad (3)$$

Here q and g are linear and nonlinear piezomagnetic coefficients, respectively, and are defined as

$$q = b\chi(M_r + \chi H_{bias}), \; g = b\chi^2 \quad (4)$$

As one can infer from Eq.(4), q is nonzero when there is either a remnant magnetization M_r or bias magnetic field. Thus, linear ME effect is present under a remnant magnetization, which is caused by the hysteresis in M vs H hysteresis. It could also be explained by hysteresis in the magnetostriction vs H [33]. On the contrary, the nonlinear (quadratic) ME effect occurs even when the bias field is zero [34,35], but its value is usually is weak compared to linear ME effect. Figure 10 shows the *H*-dependence of q obtained by differentiating the magnetostriction data in Fig. 4.

We assume that the thicknesses of magnetic and piezoelectric layers, ${}^{m}t$ and ${}^{p}t$, and the width w of the layers are much smaller than its length. The surfaces of the sample are free; therefore, the stresses on the surfaces of the plate are zero. Since the structure is thin and narrow, it can be assumed that the components of the stress T_2 and T_3 are zero not only on the surfaces, but also in the volume of the sample so that only the component of the stress tensor T_1 is nonzero. Taking into account these assumptions, we can write the equations of the strain (Hook's law) for the piezoelectric and magnetostrictive phase and equation for electric induction in the form:

$${}^{p}S_1 = \frac{1}{{}^{p}Y} {}^{p}T_1 + d_{31}E_3, \quad (5)$$

$$ {}^{m}S_1 = \frac{1}{{}^{m}Y}\,{}^{m}T_1 + q_{11}h_1, \qquad (6) $$

$$ {}^{p}D_p = \varepsilon_3 E_3 + d_{31}\,{}^{m}T_1, \qquad (7) $$

where ${}^{p}S_1$ and ${}^{m}S_1$ are the strain tensor components of the piezoelectric and magnetostrictive phases, and ${}^{p}D_3$ represents magnetic induction. The symbols ${}^{m}Y$, ${}^{p}Y$, ${}^{m}T_1$ and ${}^{p}T_1$ are the Young's modules and component of the stress tensors of the magnetic and the piezoelectric, respectively; ε_3 is the permittivity. The displacement of medium is the function of x_1, x_2 and x_3.

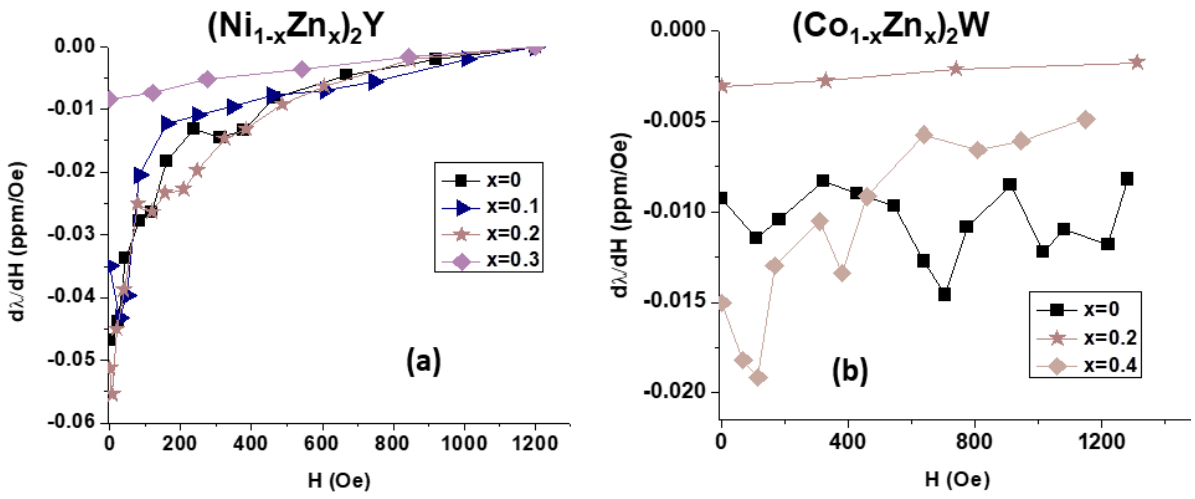

Fig.10. Field dependency of linear piezomagnetic coefficient q = dλ/dH for (a) Y- and (b) W- type hexagonal ferrites.

A noticeable change in this function occurs along the length of the composite at distances on the order of wavelength of acoustic waves. Since the wavelength for frequencies up to 100 kHz ($\lambda \cong 1$ cm) is much larger than the sample width and thickness, we can neglect any change along these directions and in the first approximation we can assume that the displacements of the medium of

the magnetic and the piezoelectric layer are equal, i.e. ${}^{m}u_1(x_1) = {}^{p}u_1(x_1) = u_1(x_1)$. Using this approximation, we can write equation of motion for the medium as

$$\bar{\rho}\frac{\partial^2 u_1}{\partial t^2} = \frac{\partial \bar{T}_1}{\partial x_1}, \tag{8}$$

where $\bar{\rho} = ({}^{m}\rho\,{}^{m}t + {}^{p}\rho\,{}^{p}t)/({}^{m}t + {}^{p}t)$, $\bar{T}_1 = ({}^{m}T_1\,{}^{m}t + {}^{p}T_1\,{}^{p}t)/({}^{m}t + {}^{p}t)$ are the average values of the density and stress tensor of the sample. Using the procedure analogous the one in Ref. 36 we get for the MEVC the following expression:

$$\alpha_E = \frac{{}^{p}Y\,{}^{p}d_{31}\,{}^{m}q_{11}}{{}^{p}\varepsilon_3\Delta}\frac{{}^{m}Y\,{}^{m}t}{{}^{m}Y\,{}^{m}t + {}^{p}Y\,{}^{p}t}\frac{tg(\kappa)}{\kappa}, \tag{9}$$

where $\Delta = 1 - K_p{}^2\left(1 - \frac{{}^{p}Y\,{}^{p}t}{{}^{m}Y\,{}^{m}t + {}^{p}Y\,{}^{p}t}\frac{tg(\kappa)}{\kappa}\right)$ is dimensionless parameter, $K_p{}^2 = \frac{{}^{p}Y({}^{p}d_{31})^2}{{}^{p}\varepsilon_3}$ where K_p is the coefficient of electromechanical coupling and $\kappa = kL/2$ dimensionless parameter, $k = \sqrt{\frac{\bar{\rho}}{\bar{Y}}}\omega$ is the wave number, and ω is the angular frequency. At low frequencies, using the fact $\kappa << 1$ and $K_p{}^2 << 1$ we get

$$\alpha_E^{Low} = \frac{{}^{p}Y\,{}^{p}d_{31}\,{}^{m}q_{11}}{{}^{p}\varepsilon_3}\frac{{}^{m}Y\,{}^{m}t}{{}^{m}Y\,{}^{m}t + {}^{p}Y\,{}^{p}t}. \tag{10}$$

For theoretical estimates we used the material parameters in Table 1. The estimated values of MEVC for $H = 0$ are shown in Fig.7 that are in very good agreement with the measured values in Fig.7. As can be inferred from Eq.(10), H-dependence of MEVC at low frequency is due to the dependence of q on H. Piezomagnetic coefficient for both $(Ni_{1-x}Zn_x)_2Y$ and $(Co_{1-x}Zn_x)_2W$ ferrites are rather large at $H_{bias} \sim 0$, and therefore MEVC also high at near zero bias magnetic field. With increasing H saturation of λ-value and $q \sim 0$ are seen for $(Ni_{1-x}Zn_x)_2Y$. It leads to the fact that

MEVC for $(Ni_{1-x}Zn_x)_2Y$ tends to zero with increasing H, in full accordance with the data in Fig. 5. For $(Co_{1-x}Zn_x)_2W$ saturation of λ is not observed for H up to 1.2 kOe and, therefore, q and MEVC have nonzero values at H up to 1.2 kOe. With increasing x the MEVC first increases, then decreases. In Fig.11 shows the dependence of MEVC vs x.

Table 1: Material parameters for hexagonal ferrites and PZT [18].

Material	**density** ρ, g/cm^3	**Young's modules** Y, GPa
Ni_2Y	5.4	154
Zn_2Y	5.46	154
Co_2W	5.31	154
Zn_2W	5.38	154
PZT	7.5	65

Frequency dependence of MEVC under an optimum bias in Fig.8 is considered next. According to Eq.(9), frequency dependency of MEVC has a resonance character. At the electromechanical resonance when the parameter $\Delta = 0$, MEVC will be maximum. The resonance frequency is determinate by

$$f_{res} \approx \frac{1}{2L}\sqrt{\frac{{}^{m}Y\,{}^{m}t + {}^{p}Y\,{}^{p}t}{{}^{m}\rho\,{}^{m}t + {}^{p}\rho\,{}^{p}t}} \quad . \tag{11}$$

Using the parameters in Table 1 we get $f_r \sim 55$ kHz. It follows from Eq.(11) that f_r will change with change in the density of composites. The composite density can be estimated from

${}^{m}\rho = (1-x)\rho_{NiY} + x\rho_{ZnY}$ for $(Ni_{1-x}Zn_x)_2Y$ ferrites and

${}^{m}\rho = (1-x)\rho_{CoW} + x\rho_{ZnW}$ for $(Co_{1-x}Zn_x)_2W$.

When x varies from 0 to 0.5, the densities of the composites change by less than 0.5% and this leads to a change in f_r by 0.05 kHz. However, a change in the sample length by $\Delta L = 1$ *mm* leads to

a change in f_r *by ~1.5 kHz* . The resonance value of MEVC α_E^{res} depends both on q and also on the Q- factor of mechanical resonance for the composite structure. The Q-factor is determined by the losses in the structures and can be taken into account by expressing the angular frequency in the form $\omega = \omega' + i\xi$, where ξ is damping coefficient. Q-factor and damping coefficient are related by the ratio $\xi = \pi f_{res} / Q$. Figure 11 shows the frequency dependency of MEVC for various lengths of composites of PZT and $(Ni_{1-x}Zn_x)_2Y$ hexagonal ferrites calculated for Q=200. This value of Q was obtained experimentally from the resonance line width using the relation $Q=f_{res}/\Delta f$, where Δf is the resonance line width. Results in Fig.11 show an order of magnitude higher peak MEVC compared to measured values in Fig.8. This difference may be due to several reasons. First, the model does not take into account the presence of epoxy layer between the ferrite and piezoelectric layers, which could significantly reduce the magnitude of ME voltage [37]. Also for calculations we used the parameters for bulk samples of ferrite and piezoelectric, which may differ from their values for thin films due to the presence of space charges at the interfaces [38-42].

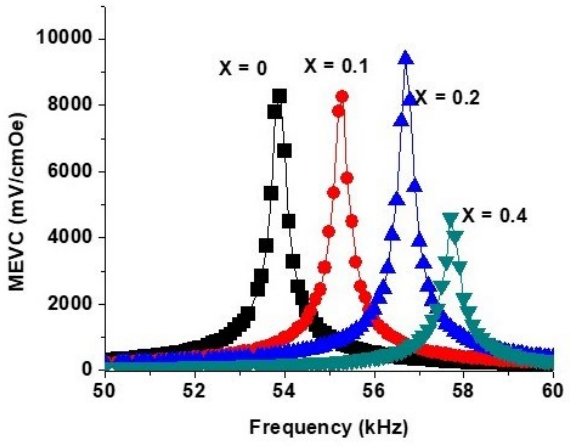

Fig.11. Frequency dependency of MEVC vs x and various length of sample for composites of PZT and $(Ni_{1-x}Zn_x)_2Y$ hexagonal ferrites

The resonance frequencies f_r in Fig.11, however, are in good agreement with the measured values. Thus there is overall agreement between the model and experiment for ME coupling under self-bias.

Results in Figs.5-8 clearly show evidence for strong ME response due to self-bias in the symmetric trilayer composites of PZT and Y- or W-type hexagonal ferrites. Composites with Y-type ferrite, in particular, have ME coefficients that are 90% or more of the values measured for optimum values of external DC bias field. Both types of composites also show a similar strong zero-bias DME effects at EMR. There have been several attempts in the past to design composites showing strong ME coupling under zero external bias as discussed in detail in Ref. 17. These included composites with either functionally graded or compositionally graded ferroic phases [43,44], exchange-bias provided, for example by an antiferromagnetic layer [45,46], utilization of hysteresis in the magnetostriction or a built-in stress [47], and non-linear ME effects [48]. In the case of composites with ferromagnetic layers that are graded in composition/magnetization, the grading was shown to lead to a built in magnetic field that could act as the bias magnetic field [40]. Grading the ferromagnetic phase with a combination of layers with positive and negative magnetostriction, such as Metglas and Ni for example, was shown to result in an ME response under zero bias [41]. Although the MEVC at low-frequency or at EMR for the system studied here are smaller than for Metglas or Ni-based composite systems [13,44], their self-bias ME characteristics are of importance for sensors and senor arrays of magnetic fields. The composites could be miniaturized for use in arrays and the strength of ME interactions could be enhanced by optimizing the ferroic order parameters for the ferrites and PZT.

5. Conclusions

The nature ME coupling in hexaferrite-ferroelectric composites has been investigated in ferrite-PZT-ferrite trilayers. Two types of hexaferrites, $(Ni_{1-x}\ Zn_x)_2$ Y and $(Co_{1-x}\ Zn_x)_2$ W with Zn concentration x = 0 to 0.4 were used. Magnetization versus static magnetic data for both types of ferrites showed a large remnant magnetization that could be attributed to uniaxial or planar magneto-crystalline anisotropy in the hexaferrites. The ME response of the composites to an applied ac magnetic field was studied at low frequencies as well as at EMR. In the case of (Ni, Zn) Y – PZT composites, the MEVC vs bias field *H* data at low frequency and MEVC vs *f* results at EMR showed evidence for strong ME interactions for zero external bias with MEVC value for *H* =0 as high as 90% of the value for optimum bias. In composites with (Co,Zn)W the zero-bias MEVC was 60-80% of the value under optimum bias at low-frequency and was 90% at EMR. A model that attributes the zero-bias ME coupling to remnant magnetization in the ferrites has been developed and estimated values of MEVC are in reasonable agreement with the data. Ferromagnetic-ferroelectric composites are of interest for use as ac magnetic field sensors in applications such as biomedical imaging. Such composites, however, may require an external magnetic bias for sensitivity enhancement. The self-biased hexaferrite-PZT composites discussed in this work constitutes a significant development for use of the composites in arrays for imaging applications.

Acknowledgments

The work at Oakland University was supported by a grant from the National Science Foundation (DMR-1808892).

References

1. N. A. Spaldin and R. Ramesh, Nature materials 18, 203 (2019).
2. M. Fiebig, T. Lottermoser, D. Meier, and M. Trassin, Nature Reviews Materials 1, 16046 (2016).
3. D. Viehland, Jie Fang Li, Yaodong Yang, Tommaso Costanzo, Amin Yourdkhani, Gabriel Caruntu, Peng Zhou et al. Journal of Applied Physics 124, 061101 (2018).
4. H. Palneedi, Venkateswarlu Annapureddy, Shashank Priya, and Jungho Ryu, Actuators, 5, 9 (2016).
5. M. M. Vopson, Critical Reviews in Solid State and Materials Sciences 40, 223 (2015).
6. Y. K. Fetisov, IEEE Sensors Journal, 14, 1817 (2014).
7. G. Srinivasan, Shashank Priya, and N. Sun. *Composite magnetoelectrics: materials, structures, and applications*. Elsevier, New York, 2015.
8. J. Wang, D. Pesquera, R. Mansell, S. van Dijken, R. P. Cowburn, M. Ghidini, and N. D. Mathur, Applied Physics Letters 114, 092401 (2019).
9. N. Ortega, Ashok Kumar, J. F. Scott, and Ram S. Katiyar. Journal of Physics: Condensed Matter 27, 504002 (2015).
10. P. Zhou, M. A. Popov, Ying Liu, Rao Bidthanapally, D. A. Filippov, Tianjin Zhang, Yajun Qi et al., Physical Review Materials 3, 044403 (2019).
11. J. van den Boomgaard, A. M. J. G. van Run, and J. van Suchtelen, Ferroelectrics 14, 727, (1976).
12. M. M. Vopson, M. M., Y. K. Fetisov, G. Caruntu, and G. Srinivasan, Materials 10, 963 (2017).

13. Y. Wang, David Gray, David Berry, Junqi Gao, Menghui Li, Jiefang Li, and Dwight Viehland, Advanced Materials 23, 4111 (2011).
14. Y. Yan, Yuan Zhou, and Shashank Priya, Applied Physics Letters 102, 052907 (2013).
15. U. Laletin, G. Sreenivasulu, V. M. Petrov, T. Garg, A. R. Kulkarni, N. Venkataramani, and G. Srinivasan, Physical Review B 85, 104404 (2012).
16. C. L. Zhang, W. Q. Chen, and Ch Zhang, Journal of Applied Physics 113, 084502 (2013).
17. Y. Zhou, Deepam Maurya, Yongke Yan, Gopalan Srinivasan, Eckhard Quandt, and Shashank Priya, Energy Harvesting and Systems 3, 1 (2016).
18. Landolt-Bornstein; *Numerical data and functional relationships in science and technology, Group III, Crystal and Solid State Physics,* vol 4(b), *Magnetic and Other Properties of Oxides*, eds. K.-H. Hellwege and A. M. Springer, Springer-Verlag, New York (1970).
19. R. C. Pullar, Progress in Materials Science 57, 1191 (2012).
20. V. L. Mathe, G. Srinivasan, and A. M. Balbashov, Applied Physics Letters 92, 122505 (2008).
21. R. Braden, I. Gordon, and R. Harvey, IEEE Transactions on Magnetics 2, 43 (1966).
22. L. M. Silber, C. E. Patton, and H. F. Naqvi, Journal of Applied Physics 54, 4071 (1983).
23. E. P. Naiden, V. A. Zhuravlev, V. I. Suslyaev, R. V. Minin, V. I. Itin, and E. Yu Korovin. International Journal of Self-Propagating High-Temperature Synthesis 20, 200 (2011).
24. F. Licci and S. Rinaldi, Journal of Applied Physics 52, 2442 (1981).
25. S. Marauska, Robert Jahns, Henry Greve, Eckhard Quandt, Reinhard Knöchel, and Bernhard Wagner, Journal of Micromechanics and Microengineering 22, 065024 (2012).
26. T. Nan, Yu Hui, Matteo Rinaldi, and Nian X. Sun, Scientific Reports 3 1985, (2013).

27. C. M. Leung, Jiefang Li, D. Viehland, and X. Zhuang, Journal of Physics D: Applied Physics 51, 263002 (2018).
28. V. Annapureddy, Miso Kim, Haribabu Palneedi, Ho-Yong Lee, Si-Young Choi, Woon-Ha Yoon, Dong-Soo Park et al., Advanced Energy Materials 6, 1601244 (2016).
29. F. Narita and Marina Fox, Advanced Engineering Materials 20, 1700743 (2018).
30. Y. Bai, Ji Zhou, Zhilun Gui, Zhensing Yue, and Longtu Li, Materials Science and Engineering: B 99, 266 (2003).
31. K. Huang, Xiansong Liu, Shuangjiu Feng, Zhanjun Zhang, Jiangying Yu, Xiaofei Niu, Farui Lv, and Xing Huang, Journal of Magnetism and Magnetic Materials 379, 16 (2015).
32. R. C. Pullar, 1999. *The synthesis and characterisation of hexagonal ferrite fibres* (Doctoral dissertation, University of Warwick).
33. Y. K. Fetisov, Dmitri D. Chashin, Nikolai A. Ekonomov, Dmitri A. Burdin, and Leonid Y. Fetisov. IEEE Transactions on Magnetics 51, no. 11 (2015): 1-3.
34. D.A. Filippov, V.M. Laletin, and T.O. Firsova, Physics of the Solid State, 56, 980 (2014).
35. Burdin D.A., Chashin D.V., Ekonomov N.A., Fetisov L.Y., Sreenivasulu G., G. Srinivasan Journal of Magnetism and Magnetic Materials, 2014, v. 358-359, p. 98-104
36. D. A. Filippov V. M. Laletin T.A. Galichyan, Applied Physics A, 115, 1087 (2014).
37. D. A. Filippov T.A. Galichyan V. M. Laletin, Applied Physics A, 116, 2167 (2014).
38. I. B. Misirlioglu M. B. Okatan S. P. Alpay, J. Appl. Phys. 108, 034105 (2010).
39. P. D. Zubko, J. Jung, and J. F. Scott. J. Appl. Phys. 100, 114112 (2006).
40. M. B. Okatan, I. B. Misirlioglu, and S. P. Alpay, Physical Review B 82, 094115 (2010).
41. I. B. Misirlioglu, G. Akcay, S. Zhong, and S. P. Alpay, J. Appl. Phys. 101, 036107 (2007).

42. J. Mangeri, Y. Espinal, A. Jokisaari, S. P. Alpay, S. Nakhmanson, and O. Heinonen, Nanoscale 9, 1616 (2017).

43. C. Sudakar, R. Naik, G. Lawes, J. V. Mantese, A. L. Micheli, G. Srinivasan, and S. P. Alpay, Appl. Phys. Lett. **90**, 062502 (2007).

44. S.K. Mandal, G. Sreenivasulu, V. M. Petrov, and G. Srinivasan, Physical Review B 84, 014432 (2011).

45. E. Lage, C. Kirchhof, V. Hrkac, L. Kienle, R. Jahns, R. Knochel, E. Quandt, and D. Meyners, Nature Materials 11, 523 (2012).

46. Menghui Li, Zhiguang Wang, Yaojin Wang, Jiefang Li, and D. Viehland, Applied Physics Letters 102, 082404 (2013).

47. Jitao Zhang, Ping Li, Yumei Wen, Wei He, Aichao Yang, and Caijiang Lu, Applied Physics Letters 103, 202902 (2013).

48. Yaojin Wang, Ying Shen, Junqi Gao, Menghui Li, Jiefang Li, and D. Viehland, Applied Physics Letters 102 , 102905 (2013).